Bio-Design and Manufacturing (2021) 4:469–478
https://doi.org/10.1007/s42242-021-00131-w

RESEARCH ARTICLE

Electrospun fiber membrane with asymmetric NO release for the differential regulation of cell growth

Shengyu Chen[1,4] · Fan Jia[2] · Luying Zhao[3] · Fuyu Qiu[1,4] · Shaohua Jiang[3] · Jian Ji[2] · Guosheng Fu[1,4]

Received: 2 December 2020 / Accepted: 13 March 2021 / Published online: 24 April 2021

Abstract

The high incidence of cardiovascular disease has led to significant demand for synthetic vascular grafts in clinical applications. Anti-proliferation drugs are usually loaded into devices to achieve desirable anti-thrombosis effects after implantation. However, the non-selectiveness of these conventional drugs can lead to the failure of blood vessel reconstruction, leading to potential complications in the long term. To address this issue, an asymmetric membrane was constructed through electrospinning techniques. The bilayer membrane loaded and effectively released nitric oxide (NO), as hoped, from only one side. Due to the short diffusion distance of NO, it exerted negligible effects on the other side of the membrane, thus allowing selective regulation of different cells on both sides. The released NO boosted the growth of endothelial cells (ECs) over smooth muscle cells (SMCs)—while on the side where NO was absent, SMCs grew into multilayers. The overall structure resembled a native blood vessel, with confluent ECs as the inner layer and layers of SMCs to support it. In addition, the membrane preserved the normal function of ECs, and at the same time did not exacerbate inflammatory responses. By preparing this material type that regulates cell behavior differentially, we describe a new method for its application in the cardiovascular field such as for artificial blood vessels.

Graphic abstract

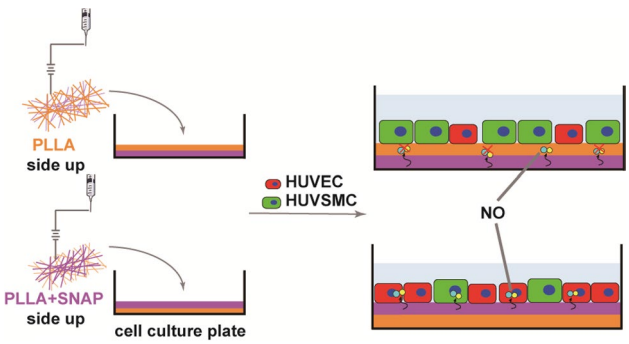

Keywords Nitric oxide · Asymmetric drug release · Electrospun fiber membrane · Artificial blood vessel

✉ Shaohua Jiang
shaohua.jiang@njfu.edu.cn

✉ Jian Ji
jijian@zju.edu.cn

✉ Guosheng Fu
fugs@zju.edu.cnAuthors and Affiliations

[1] Department of Cardiology, Sir Run Run Shaw Hospital, Zhejiang University School of Medicine, Hangzhou 310016, China

[2] MOE Key Laboratory of Macromolecule Synthesis and Functionalization, Department of Polymer Science and Engineering, Zhejiang University, Hangzhou 310027, China

[3] Co-Innovation Center of Efficient Processing and Utilization of Forest Resources, College of Materials Science and Engineering, Nanjing Forestry University, Nanjing 210037, China

[4] Key Laboratory of Cardiovascular Intervention and Regenerative Medicine of Zhejiang Province, Hangzhou 310016, China

Introduction

Cardiovascular disease (CVD) remains the leading cause of death worldwide [1, 2]. When a part of a blood vessel loses function due to disease, damage, or aging, a vascular transplant is required. Because of the strong rejection of allogeneic organs and few sources for them, artificial blood vessels have become an alternative. Although they provide sufficient mechanical strength, polymer-based synthetic monolayer vascular grafts [3] still have limited resistance to surface thrombosis [4], which may lead to restenosis after implantation. The multilayer structure of healthy blood vessels ensures a perfect combination of good physical and mechanical properties with anticoagulant properties. The ideal artificial blood vessel should be designed to imitate these multi-layered characteristics in order to obtain a structure more in line with normal vessels.

Vascular restenosis is composed mainly of hyper-proliferative smooth muscle cells (SMCs), inflammatory cells, and platelets. The current treatment of vascular stenosis is to inhibit cell proliferation. The representative drugs rapamycin and paclitaxel have no selectivity in exerting inhibitory effects. They block the proliferation of SMCs as well as endothelial cells (ECs). This process leads to incomplete endothelialisation, which can further aggravate stenosis [5, 6]. A complete intimal layer composed of ECs is necessary for maintaining blood vessel health and smooth blood flow. Therefore, the ideal anti-stenotic drug needs to inhibit the proliferation of SMCs and the progress of inflammation, while ensuring the integrity and functions of ECs.

Nitric oxide (NO) provides the possibility of regulating cells differently. NO is a biological effector that plays an important role in vasodilation, endothelial function, and other vascular processes [7]. Previous studies have shown that NO can strongly inhibit the proliferation of SMCs [8–12] and resist platelet aggregation [13] and leukocyte adhesion, while improving endothelial cell function at low doses [14]. Therefore, NO can be used as a selective anti-stenosis drug. However, anti-stenotic drugs generally act solely on the intima of blood vessels. An ideal vascular transplantation requires that the SMCs in the outer layer have their growth space, ensuring that the graft has sufficient mechanical strength and good vascular compliance after transplantation.

Electro-spinning technology is an emerging technique for constructing biomedical scaffolds. By employing a spinning polymer solution under high voltage static electricity, it can control different material components to prepare nanofiber meshes with controllable structures [15]. It can provide flexible design by adjusting fiber diameter, porosity, texture, and pattern formation [16], offering possibilities for the design of multifunctional structural materials [17]. In many studies, electro-spinning technology has been applied to the heart. For example, using multi-channel and coaxial electrospinning technology to prepare an outer sheath of the great saphenous vein can effectively inhibit the formation of new intima and achieve controlled drug release [18]. By controlling different pore sizes [19] or combining cytokines [20], artificial blood vessels with bilayer electrospun fiber membranes have been reported to selectively control the growth of different cells. However, achieving an asymmetric growth of cells on a bilayer vascular graft in a feasible but simple manner remains a lasting challenge.

In this study, we used *S*-Nitroso-*N*-acetyl-DL-penicillamine (SNAP) loaded electropsun fiber membranes to achieve the asymmetric release of NO. Taking advantage of the short release distance of NO [21, 22], only the area near the drug-loaded side of the bilayer membrane has sufficient NO concentration. First, we verified the differential regulation of the growth of ECs and SMCs by a SNAP-loaded monolayer membrane. Then we co-cultured ECs and SMCs on the bilayer membrane. This asymmetric structure made cell growth more consistent with the natural vascular structure: the SNAP-incorporated side of the membrane guarantees endothelial growth while inhibiting SMC proliferation to prevent thrombosis, while the other side without SNAP makes SMCs grow naturally to form a vascular elastic layer (Fig. 1). This asymmetric structure that constructs a differential regulation of cell behaviors provides new ideas for applications in the cardiovascular field such as in artificial blood vessels.

Results

Characterization of SNAP-PLLA nanofibers

We mixed a solution of SNAP and poly(L-lactide) (PLLA) to fabricate the nanofibers. Images taken by a scanning electron microscope (SEM) indicated the successful preparation of a uniform and porous nanofiber membrane (Figs. 2a and S1b). The nanofiber diameters of pure PLLA and PLLA-SNAP mixtures were 1.710 ± 0.314 μm (PLLA) and 450 ± 48 nm (PLLA + SNAP), respectively (Fig. 2b). Sulfur analysis was measured by energy-dispersive spectrum (EDS). A clear peak between 2.3 and 2.4 keV was observed, which is typical of the sulfur element (Fig. S1a). The average pixel areas of sulfur element analysis showed that the SNAP electrospun membrane had a significantly higher sulfur content than the blank membrane (Fig. 2c). The thicknesses of the pure PLLA and PLLA-SNAP mixtures were 285.5 ± 2.2 μm and

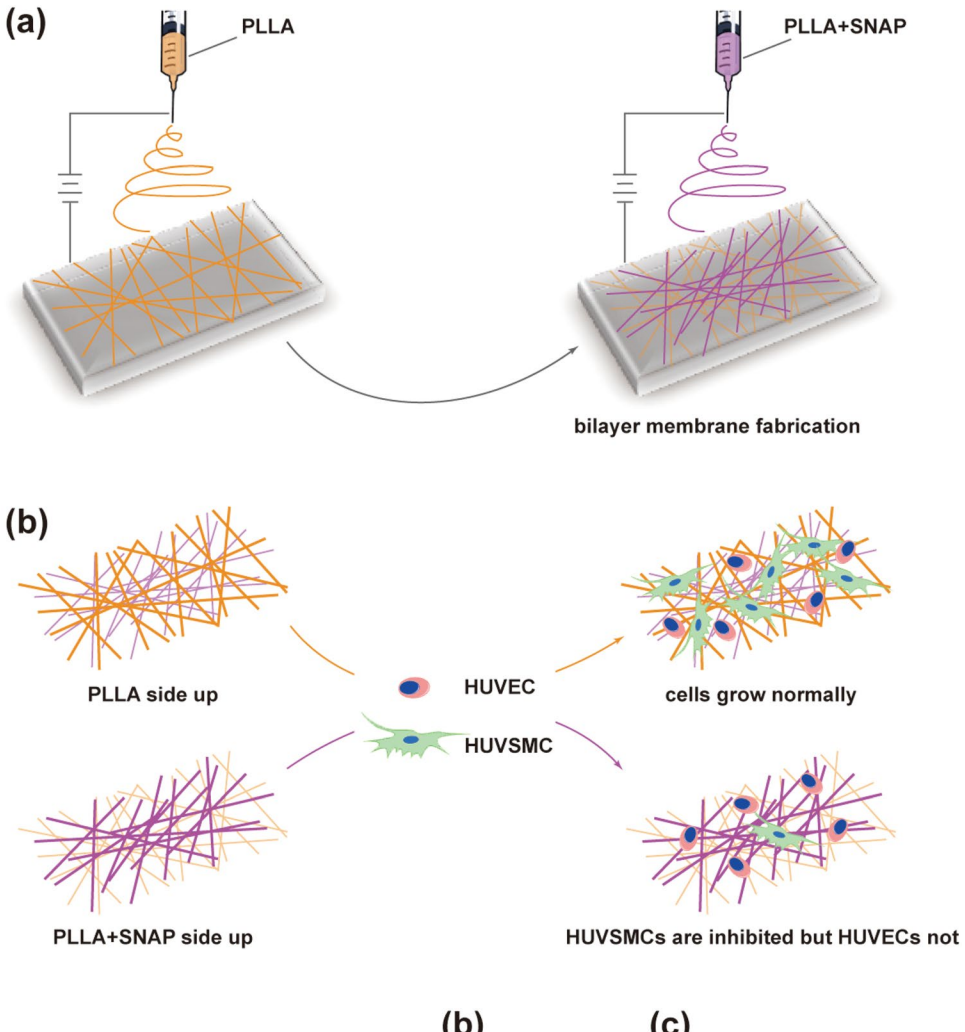

Fig. 1 Schematic design of experiment. **a** Fabrication of a bilayer electrospun membrane by electro-spinning technology; **b** when HUVECs and HUVSMCs were co-cultured on both sides of the bilayer membrane, cells grew normally on the PLLA side; while on the PLLA + SNAP side, the growth of HUVSMCs was significantly inhibited. However, HUVECs still grew normally

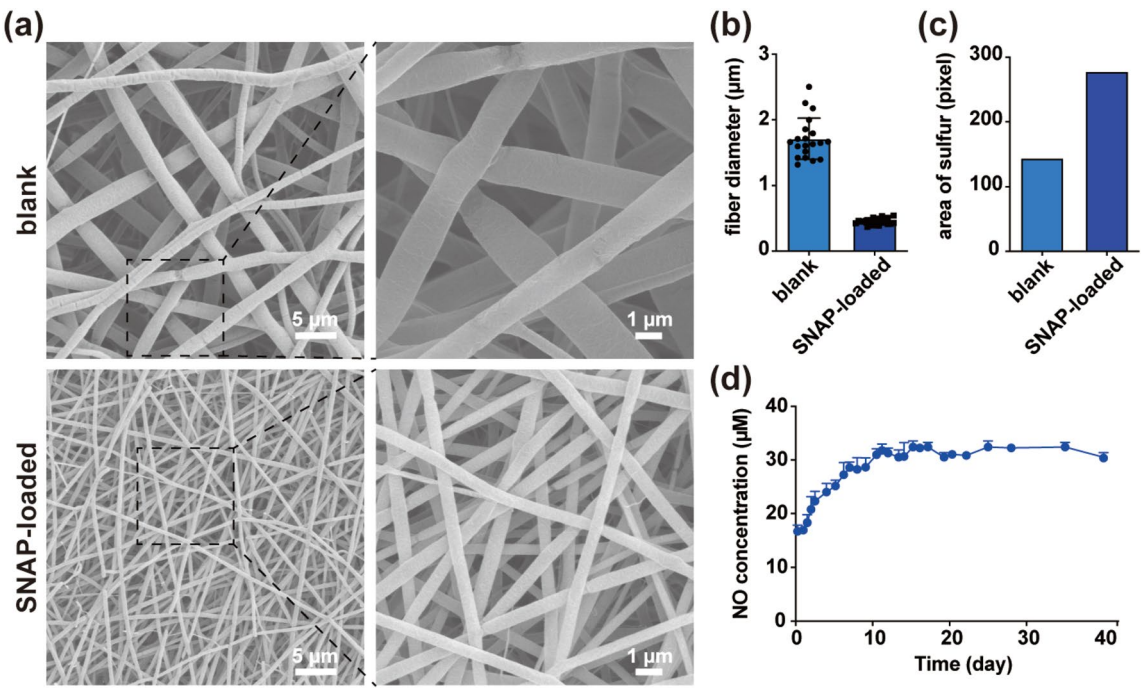

Fig. 2 Characterization of electrospun fiber membrane. **a** SEM images of the electrospun fiber membrane; **b** average diameters of nanofibers; **c** average pixel areas of sulfur element analysis from EDS; **d** NO releasing profile of the SNAP-loaded electrospun fiber membrane

284.8 ± 2.8 μm, respectively, and there was no significant difference in thickness between the two films (Fig. S1d).

NO release of SNAP-loaded fiber membranes

A slow and continuous NO release was achieved by incorporating SNAP into electrospinning. SNAP was loaded into the nanofibers 10 wt.% relative to PLLA concentrations. The average weight of each electrospun membrane pad was 1.23 mg, the average SNAP content per pad was 0.123 mg, and the average drug concentration of per well was 140 μM. Each mole of SNAP donor released 1 mol of NO. Figure 2d shows that the amount of NO released slowly increased to about 30 μM in about one week. The membrane maintained a stable release of effective concentration (about 1/5–1/4 of the content) for at least 40 d or longer.

Biocompatibility of electrospun fiber membranes

To determine the biocompatibility of electrospun fiber membranes, we compared the difference in cell growth on membranes, TCPS, and glass slides (Fig. S2). When cells were incubated on the surfaces of different materials, after incubating for 24 h and 48 h, cell growth on the electrospun fiber membrane was slightly lower than that on TCPS but was almost the same as that on glass slides (Fig. S2b). We then used the cell counting method and CCK-8 kit to measure the time gradients of cell number (Fig. S2c) and cell viability (Fig. S2d), respectively. The cell viability of HUVECs and HUVSMCs on the electrospun membrane was slightly inferior to that on TCPS. While the absolute value of the cell count gradually increased with time, this indicates

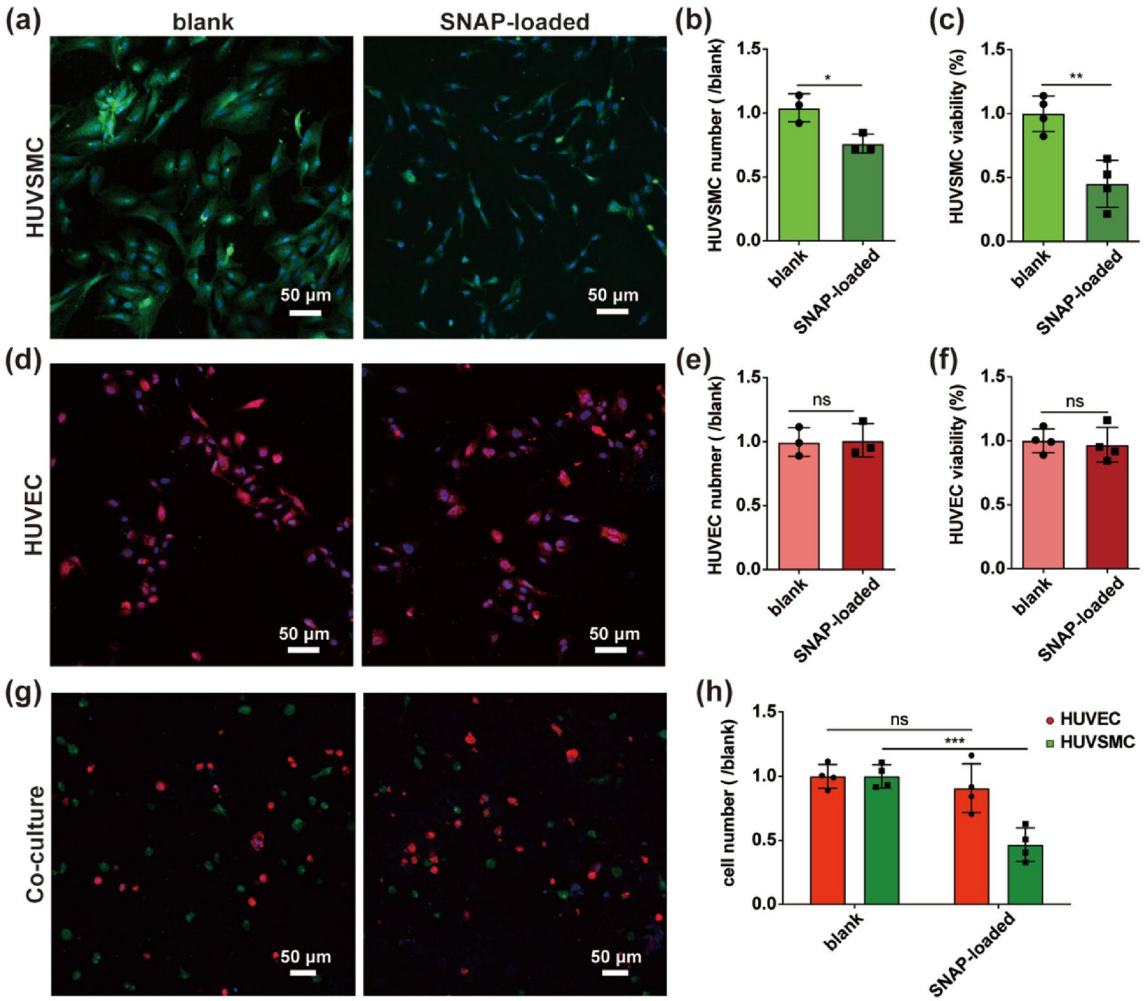

Fig. 3 Effect of the electrospun fiber membrane on the proliferation of HUVEC and HUVSMC. Immunofluorescent images (**a**) and statistical diagrams (**b**) of differential effects of electrospun membranes on HUVSMC, **c** cell viability of HUVSMC on different membranes. Immunofluorescent images (**d**) and statistical diagrams (**e**) of differential effects of electrospun membranes on HUVEC, **f** cell viability of HUVEC on different membranes. Immunofluorescent images (**g**) and statistical diagrams (**h**) of co-culture of HUVEC and HUVSMC (red: HUVEC; green: HUVSMC; blue: Nucleus)

that the electrospun membrane provided an environment for stable cell proliferation.

Proliferation of ECs and SMCs on electrospun fiber membranes

HUVECs and HUVSMCs were seeded separately on both blank and SNAP-loaded electrospun membranes to evaluate cell viability after 48 h. The figures show that there was no significant difference in HUVEC proliferation between the SNAP-loaded and the blank membrane (Fig. 3d–3f). However, HUVSMCs demonstrated a significant difference in growth on various membranes (Figs. 3a–3c, S3). Changes between confocal and SEM pictures were consistent with the results of cell viability. Obvious morphological changes of SMCs were observed on the SNAP-loaded membrane (Fig. 3a). Then, HUVECs and HUVSMCs were co-cultured on the SNAP-loaded side of the membranes. While the growth of HUVECs was not affected, significant inhibition of the proliferation of HUVSMCs was observed (Fig. 3g and 3h). This indicated the selective effect of the SNAP-loaded electrospun membrane on cells.

EC and SMC functions on electrospun fiber membranes

Figure 4 shows the functions of cells on electrospun fiber membranes. First, we detected the relative RNA contents of VCAM-1, ICAM-1, MCP-1, IL-1β, IL-6, and IL-8 in our experiments, covering most of the pathological processes of atherosclerosis including leukocyte adhesion, infiltration, and plaque development. The relative RNA contents of cells grown on electrospun fiber membranes showed no significant differences compared to cells in normal conditions (Fig. 4c).

The earliest pathological process of atherosclerosis is impaired vasodilation mediated by endothelium, and so diastolic function and EC function were tested. Diastolic function represented by SMCs was determined by ELISA assay. It revealed that the amount of cGMP content showed a significant rise when incubated on SNAP-loaded membranes (Fig. 4a). EC function was represented by the amount of NO secreted from ECs. Figure 4b shows that the amount of NO increased in cells seeded on the SNAP-loaded electrospun membrane.

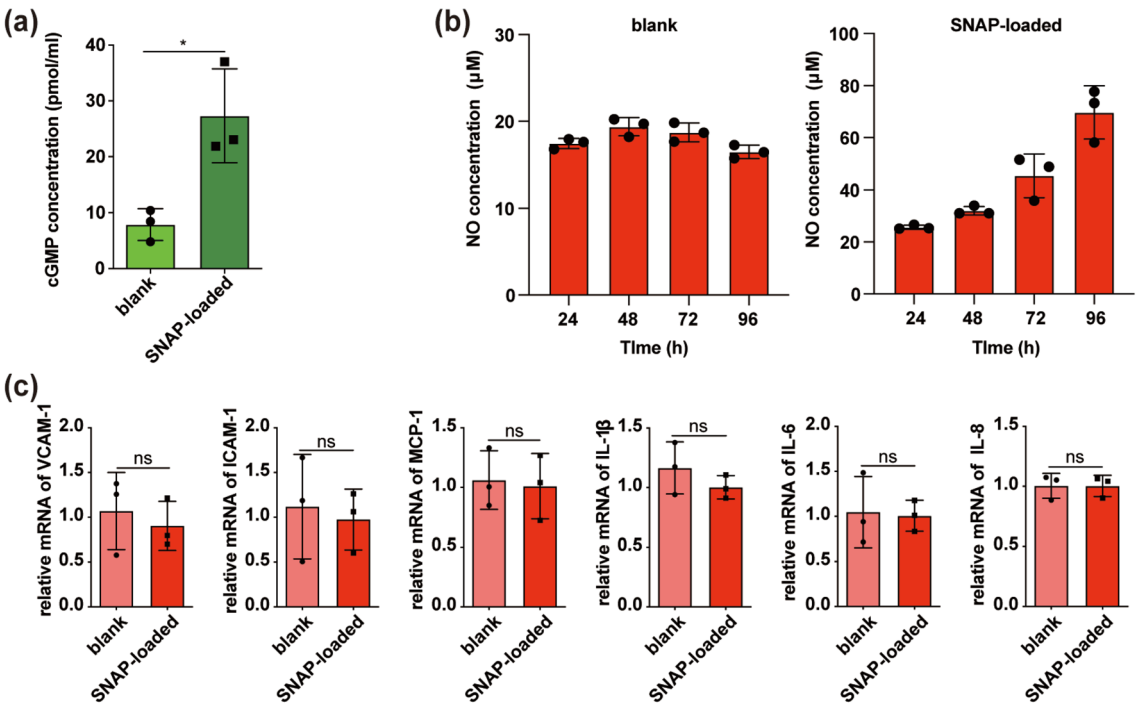

Fig. 4 Effects of electrospun fiber membrane on functions of HUVEC and HUVSMC. **a** cGMP concentration of HUVSMC on different electrospun membranes; **b** NO release from HUVEC on different electrospun membranes (left: HUVEC on blank membrane, right: HUVEC on SNAP-loaded membrane); **c** Relative mRNA expression of endothelial cell adhesion molecules and inflammatory factors on different electrospun membranes

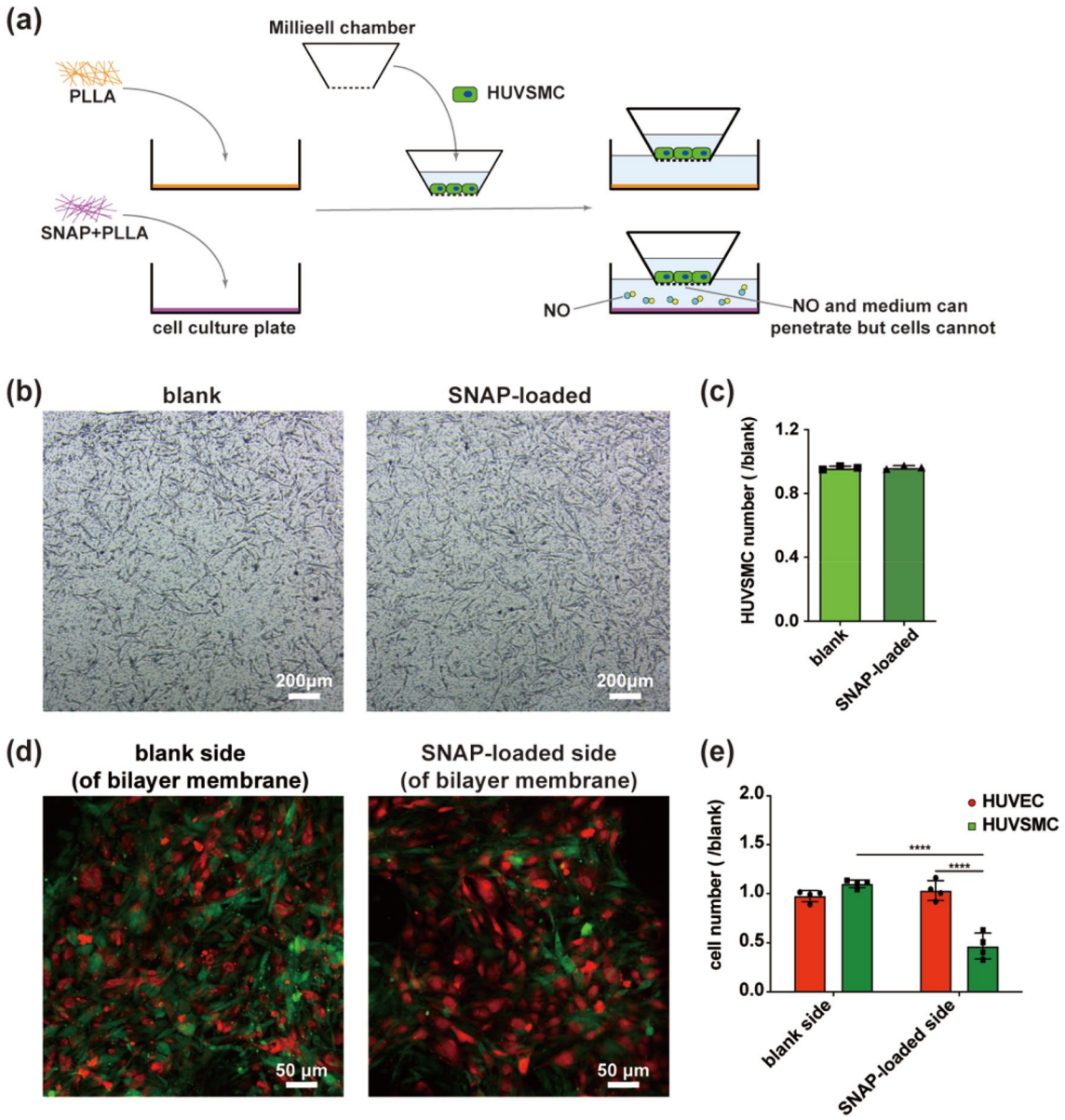

Fig. 5 Effect of bilayer electrospun fiber membrane on co-culture of HUVEC and HUVSMC. **a** Schemes of experiment set-ups of the Millieell chamber: HUVSMCs were seeded into Millieell chambers, the chambers were placed into cell culture plates, cells and membrane were separated but NO and medium could pass through both sides of the membrane. Optical microscope images (**b**) and statistical diagrams (**c**) of HUVSMC on different electrospun membranes. Immunofluorescent images (**d**) and statistical diagrams (**e**) of HUVEC and HUVSMC on different sides of the bilayer electrospun membranes (red: HUVEC, green: HUVSMC)

Co-culture of ECs and SMCs on bilayer electrospun fiber membranes

In order to rule out the influence of SNAP on cells growing contralaterally, we used Millieell chambers to prevent the direct contact between cells and membrane (Fig. 5a). Images observed with an optical microscope showed no significant difference of SMC proliferation between the two groups (Fig. 5b and 5c). This shows that when separated from direct contact between cells and membrane, cell growth is not affected by SNAP loaded in the electrospun membrane. We then prepared a bilayer electrospun fiber membrane loaded with 10 wt.% SNAP on the inner side and only PLLA on the outer side (Fig. S1c) and then co-cultured two types of cells on both sides. Confocal pictures showed that on the side loaded with SNAP, the proliferation of HUVSMCs was significantly suppressed, while HUVECs were not affected. On the outer side of the bilayer membrane, the proliferation of HUVSMCs was not affected by the secretion of NO from the inner side, and cells had formed an overlapping cell layer (Fig. 5d and 5e).

Discussion

The main purpose of our experiment was to build a double-layer asymmetric structure similar to natural blood vessels—the inner layer maintains the activity of ECs and inhibits the proliferation of SMCs; the outer layer provides sufficient space for SMC growth. This structure can ensure the integrity of ECs in the inner wall of the blood vessel, exerting anticoagulation and anti-platelet aggregation to suppress the occurrence of long-term restenosis [23], while SMCs grow into an overlapping structure on the outer layer to build a vascular elastic layer [24], providing compliance and mechanical strength of the blood vessel and secreting ECM to enable ECs grow continuously and stably (Fig. 1). Therefore, we chose as the material in our experiment the electrospun membrane which can be freely adjusted with different pore sizes and thicknesses, so that cells could grow into an overlapping structure on the membrane. NO was chosen as the drug and doped into the inner layer of the bilayer electrospun membrane because of its selective effect on the growth of SMCs and ECs. The proliferation of SMCs grown on the inner layer was selectively inhibited.

In the cardiovascular system, NO is a physiological vasodilator that can convey vascular protection in various ways. NO is significantly active and degrades in seconds. Nitrosoglutathione (GSNO) is the pathway of NO release and transport in the human body. Its SNO group can be decomposed into NO and synthesized from NO in seconds [25, 26]. SNAP contains the same SNO group as GSNO and can release NO spontaneously under physiological conditions [27]. As a derivative of amino acids, SNAP is widely recognized for its lack of tolerance [11, 28], which is usually observed in the long-term use of nitroglycerin [29]. Considering these advantages, we chose SNAP as NO donors to fabricate NO-releasing nanofibers. As shown in Figs. 2 and S1, PLLA nanofibers with and without SNAP doped were uniform in diameter, demonstrating the strong maneuverability of electro-spinning processes. Compared with fibers of pure PLLA, the smaller size of PLLA-SNAP fibers is likely due to the reduced viscosity of the PLLA solution by the plasticization of SNAP. On the surface of the electrospun membrane, different kinds of cells grow similarly, and cells can successfully adhere and stably proliferate. The appearance of a peak corresponding to the sulfur element in EDS indicates the successful embedment of SNAP in PLLA nanofibers (Fig. S1a). SNAP-embedded fibers could continuously release NO for at least 40 d, much longer than SNAP in solution (Fig. 2d). The controlled-release ability is highly desirable in many scenarios, including in artificial blood vessel [30]. Membranes loaded with SNAP still have the function of NO; that is, they are selective for the proliferation of ECs and SMCs. We have demonstrated it in the experiments by separately culturing and co-culturing two kinds of cells (Fig. 3).

The formation of stenosis in blood vessels is a complex inflammatory process. Impaired endothelial function is the initial change, manifested by reduced NO released from ECs. NO is a vasodilator. Under physiological conditions, NO diffused into SMCs can act on smooth muscle receptor soluble guanosyl cyclase (sGC), catalyze cyclic guanosine monophosphate (cGMP) to start the process of vessel relaxation and inhibit SMC proliferation [31]. Reduced NO release from ECs facilitated attenuation of NO-sGC-cGMP signaling, causing the failure of the normal relaxation of SMCs. This might increase the tension of blood vessel and exacerbate local stenosis [32]. In our experiment, we detected the content of NO released by ECs and the content of cGMP in SMCs to assess the endothelial early damage [33], Fig. 4 shows that a SNAP-loaded membrane can alleviate the reduced release of NO caused by the injured endothelial and promote smooth muscle relaxation. The increase in cGMP in SMCs on SNAP-loaded membranes compensated the NO loss due to EC incompleteness, maintaining normal functions similar to those of native blood vessels [34].

When ECs were injured, the monocytes moved closer to the blood vessel wall, and the vascular cell adhesion molecule 1 (VCAM-1) and intercellular adhesion molecule 1 (ICAM-1) expressed by ECs then fixed monocytes in the EC lesion location [35]. ECs can produce monocyte chemoattractant protein 1 (MCP-1) and IL-8 under the action of oxidizing factors. MCP-1 can promote the migration of bound monocytes to the arterial wall [36]. As the disease progresses, EC secreted IL-1β and TNF-α, thereby promoting IL-6 secretion. IL-6 can cause plaque instability and increase the risk of illness. The formation of atherosclerotic lesions is a complex process of immune regulation [37]. The relative RNA content of inflammatory cytokines, such as VCAM-1, ICAM-1, MCP-1, IL-1β, IL-6, and IL-8, clearly demonstrates that electrospun membranes do not cause an increase in inflammation and aggravation of disease as a potential implanted component.

Although NO has a very strong ability to regulate various physiological processes, NO also has the shortcoming of a short action distance and easy inactivation after release. Its effect is usually limited to the production site. However, this also provides an opportunity to use NO in an asymmetric structure to selectively manipulate cell behavior. We took advantage of this shortcoming to prepare a bilayer electrospun membrane. In normal incubation and co-culture experiments, as shown in Fig. 5, the side of the bilayer electrospun membrane had a significant effect on ECs and SMCs. The bilayer membrane promoted EC growth on the SNAP load side, while the blank PLLA side maintained SMC growth, which promoted a structure similar to natural blood vessels. These effects have also been verified on single-layer films.

Materials and methods

Preparation of blending nanofibers

The concentrations of all solution components and solutions are given on a wt/wt basis. A 10 wt.% poly(L-lactide) (PLLA, REVODE 190, HISUN, China) solution was prepared by dissolving PLLA resin in 1,1,1,3,3,3-hexafluoroisopropanol (HFIP, 99%, JACS, China) at room temperature, stirring at 500 r/min for 8 h. The PLLA solution was mixed with SNAP (10 wt.% relative to PLLA concentrations) in the same condition (500 r/min for 8 h) for electrospinning. The electro-spinning conditions were described as following. A metal disk was used to collect electro-spinning nanofibers. A plastic syringe with a 12-mm needle containing 2 mL of solution was placed on a syringe pump at a flow rate of 1 mL/h. The collecting distance between the spinneret and the receiving device was 15 cm. The membrane was cut into small pads with diameters of 0.75 cm according to the well size of the 24-well plate, soaked in 75% alcohol for 30 min, washed three times with PBS, and dried for use.

Cell culture

HUVECs were cultured in an endothelial cell medium (ECM) with 5% fetal bovine serum, a 1% endothelial cell growth supplement, and a 1% penicillin/streptomycin solution (ScienCell Research Laboratories, Carlsbad, CA, USA). HUVSMCs were cultured in a smooth muscle cell medium (SMCM) with 2% fetal bovine serum, 1% endothelial cell growth supplement, and a 1% penicillin/streptomycin solution (ScienCell Research Laboratories, Carlsbad, CA, USA). The cells were purchased from ScienCell Research Laboratories and incubated at 37 °C under 5% CO_2 atmosphere. Cells between passages 4–7 were used in this experiment.

Cell number and cell viability

To determine the effect on cell proliferation, cells were seeded at a density of 5000 per well in 24-well plates and cultured for different lengths of time. Cell proliferation was measured by cell number and cell viability. Cell number was determined by the dissociation of adherent cells with trypsin and counting with a microscope. Cell viability was detected with the Cell Counting Kit-8 (CCK-8) (Dojindo, Tokyo, Japan). Add 20 μL CCK-8 solution with a total volume of 200 μL of serum-free medium to each well. After 1–3 h of incubation at 37 °C, the absorbances were measured at 450 nm. Cell viability was determined using the equation below:

$$\text{Cell viability (\%)} = \text{Absorbance (treated cells)}/\text{Absorbance (control cells)} \times 100\%.$$

NO release measurement

The SNAP-loaded electrospun fiber membrane pads were first weighed to calculate the SNAP content. The pads were put into 24-well plates, serum-free Dulbecco's modified eagle medium (DMEM) was added and they were placed in a 37 °C incubator. The DMEM was collected at different time points. NO release was quantified by the Nitric Oxide Test Kit (Beyotime, Shanghai, China) according to the manufacturer's instructions.

Millieell chambers were used to test the effect of long-distance release of NO from SNAP-loaded membranes on cells. The membranes were placed in 24-well plates. HUVSMCs were seeded into the Millieell Chambers (Millipore Corp., Bedford, MA, USA). The chambers were inserted into wells. The medium in the wells covered the bottom of the chambers (Fig. 5a). Direct contact between the cells and electrospun membranes was prevented in this way. After 48 h, the medium was removed and the bottom of the chamber was gently wiped with a cotton swab. The cells were fixed with paraformaldehyde and stained with crystal violet dye. The membrane was cut off at the bottom of the chamber and observed with an optical microscope.

Image acquisition with a scanning electron microscope

The cells were first dehydrated. The cells were fixed with paraformaldehyde and configured to a volume fraction of 20%–100% alcohol with a gradient of 10%. The cells were treated with a 20% alcohol solution for 5 min, then the solution was aspirated, and the cells were treated with a 30% alcohol solution for another 5 min and so on until the last 5 min with the absolute ethanol treatment. The alcohol was removed and the cells were dried. The cells were observed by a Nikon scanning electron microscope.

Immunofluorescence staining and image analysis

HUVECs and HUVSMCs planted on the electrospun fiber membrane were stained for 2 h by adding rabbit anti-human von Willebrand factor (anti-vWF) monoclonal antibody (1:500, Invitrogen, CA, USA) or anti-calponin (1:500, Invitrogen, CA, USA), respectively, before being detached from the cultural dishes. The cells were Isolated and seeded into 24-well plates. After 48 h, the cells were observed by a Nikon fluorescence microscope. The images were generated by collecting each image of the Z-stack and by projecting pixel intensity onto one single image.

cGMP analysis

HUVSMCs were incubated for 48 h under different treatments. The cGMP secretion of HUVSMCs was measured by the cGMP ELISA kit (Enzo Life Sciences, New York, USA) according to the manufacturer's instruction. In brief, standards or samples were added into the plate provided with the kits. The conjugate and antibody were added into the appropriate wells. After incubation at room temperature for 2 h, the contents of the wells were emptied and washed 3 times, then pNpp substrate solution was added to every well. The cells were incubated at room temperature for another 1 h. The stop solution was added and the absorbances at 405 nm were immediately read. A Logit-Log paper was used to draw the binding percentage of the standard and the cGMP concentration. The line passing through these points approximated the fitting curve. The cGMP concentration in the sample could be determined by interpolation.

Relative RNA content measurement by qPCR

Total RNA was isolated by using the TRIzon reagent (CWBIO, Beijing, China), following the manufacturer's instructions. To synthesize cDNA, the PrimeScript RT-PCR kit (Takara, Dalian, China) was used. All PCR reactions were run with an UltraSYBR Mixture (CWBIO, Beijing, China) and primers. qPCR was performed following the manufacturer's instructions. The average threshold cycle values (Ct) from the PCR reactions were normalized to GAPDH to achieve the ΔCt value. The ΔCt values of the experimental set were normalized to control and set to achieve the ΔΔCt value. The $2^{-\Delta\Delta Ct}$ value was used as the reported data for analysis.

Statistical analysis

The experiments were performed in triplicate at a minimum. Data obtained from the experiments were statistically analyzed using *GraphPad* with ANOVA or Student's *t* test. The probability value of $p < 0.05$ was considered significant.

Conclusions

In summary, electrospun fiber membrane shows strong biocompatibility with multiple cells. Embedment of NO donor SNAP slows NO release. By utilizing the short diffusion distance of NO, simultaneous regulation of ECs and SMCs on different sides of a membrane was achieved by constructing an asymmetric structure. The SNAP-loaded side inhibited proliferation and improved the relaxation of SMCs, while enhancing the proliferation and normal functions of ECs. On the other side, SMCs quickly overgrew ECs to form overlapping cell layers, due to a lack of sufficient NO. Therefore, a Janus structure, similar to those of native blood vessels, was easily achieved. In addition, the membrane did not promote undesired inflammation. This strategy may hold strong promise for other future research into fabricating blood vessels.

Supplementary Information The online version contains supplementary material available at https://doi.org/10.1007/s42242-021-00131-w.

Acknowledgements This work was supported by the Natural Key Research and Development Project of Zhejiang Province, China (No. 2018C03015), the National Key Research and Development Program of China (No. 2016YFC1102203), and the Medical Health Science and Technology Projects of Zhejiang Province (No. 2019KY426).

Author contributions SYC and FJ contributed to conceptualization; SYC and LYZ were involved in methodology; FJ contributed to investigation; SYC was involved in writing-original draft; all authors contributed to writing-review and editing; FYQ, JJ, GSF were involved in funding acquisition; SHJ, JJ, GSF contributed in resources; SHJ, JJ, GSF were involved in supervision.

Declarations

Conflict of interest The authors declare that there is no conflict of interest.

Ethical approval This article does not contain any studies with human or animal subjects performed by any of the authors.

References

1. PrimeView (2019) Atherosclerosis. Nat Rev Dis Primers 5(1):57. https://doi.org/10.1038/s41572-019-0116-x
2. Serruys PW, de Jaegere P, Kiemeneij F et al (1994) A comparison of balloon-expandable-stent implantation with balloon angioplasty in patients with coronary artery disease. N Engl J Med 331:489–495. https://doi.org/10.1056/NEJM199408253310801
3. Ren X, Feng Y, Guo J et al (2015) Surface modification and endothelialization of biomaterials as potential scaffolds for vascular tissue engineering applications. Chem Soc Rev 44(15):5745. https://doi.org/10.1039/C4CS00483C
4. Li S, Sengupta D, Chien S (2014) Vascular tissue engineering: from in vitro to in situ. Wiley Interdiscip Rev Syst Biol Med 6(1):61–76. https://doi.org/10.1002/wsbm.1246
5. Angiolillo DJ, Sabata M, Alfonso F, Macaya C (2004) "Candy wrapper" effect after drug-eluting stent implantation: déjà vu or stumbling over the same stone again? Catheter Cardiovasc Interv 61(3):387–391. https://doi.org/10.1002/ccd.10765
6. Kang SJ, Mintz GS, Akasaka T et al (2011) Optical coherence tomographic analysis of in-stent neoatherosclerosis after drug-eluting stent implantation. Circulation 123(25):2954–2963. https://doi.org/10.1161/CIRCULATIONAHA.110.988436
7. Divakaran S, Loscalzo J (2017) The role of nitroglycerin and other nitrogen oxides in cardiovascular therapeutics. J Am Coll Cardiol 70(19):2393–2410. https://doi.org/10.1016/j.jacc.2017.09.1064
8. Bauer JA, Fung HL (1991) Differential hemodynamic effects and tolerance properties of nitroglycerin and an S-nitrosothiol

in experimental heart failure. J Pharmacol Exp Ther 256(1):249–254. https://doi.org/10.0000/PMID1899118
9. Garg UC, Hassid A (1989) Nitric oxide-generating vasodilators and 8-bromo-cyclic guanosine monophosphate inhibit mitogenesis and proliferation of cultured rat vascular smooth muscle cells. J Clin Invest 83(5):1774–1777. https://doi.org/10.1172/JCI114081
10. Kowaluk EA, Fung HL (1990) Spontaneous liberation of nitric oxide cannot account for in vitro vascular relaxation by S-nitrosothiols. J Pharmacol Exp Ther 255(3):1256–1264
11. Kowaluk EA, Poliszczuk R, Fung HL (1987) Tolerance to relaxation in rat aorta: comparison of an S-nitrosothiol with nitroglycerin. Eur J Pharmacol 144(3):379–383. https://doi.org/10.1016/0014-2999(87)90392-x
12. Shaffer JE, Han BJ, Chern WH, Lee FW (1992) Lack of tolerance to a 24-hour infusion of S-nitroso N-acetylpenicillamine (SNAP) in conscious rabbits. J Pharmacol Exp Ther 260(1):286–293. https://doi.org/10.1002/jps.2600810124
13. Lindkvist M, Fernberg U, Ljungberg LU et al (2019) Individual variations in platelet reactivity towards ADP, epinephrine, collagen and nitric oxide, and the association to arterial function in young, healthy adults. Thromb Res 174:5–12. https://doi.org/10.1016/j.thromres.2018.12.008
14. Shen YH, Wang XL, Wilcken DE (1998) Nitric oxide induces and inhibits apoptosis through different pathways. FEBS Lett 433(1–2):125–131. https://doi.org/10.1016/S0014-5793(98)00844-8
15. Ahmed FE, Lalia BS, Hashaikeh R (2015) A review on electrospinning for membrane fabrication: challenges and applications. Desalination 356:15–30. https://doi.org/10.1016/j.desal.2014.09.033
16. Mo XM, Xu CY, Kotaki M, Ramakrishna S (2004) Electrospun P(LLA-CL) nanofiber: a biomimetic extracellular matrix for smooth muscle cell and endothelial cell proliferation. Biomaterials 25(10):1883–1890. https://doi.org/10.1016/j.biomaterials.2003.08.042
17. Burger C, Hsiao BS, Chu B (2006) Nanofibrous materials and their applications. Annu Rev Mater Res 36:333–368. https://doi.org/10.1146/annurev.matsci.36.011205.123537
18. Zhang Y, Fang Q, Niu K et al (2019) Time-dependently slow-released multiple-drug eluting external sheath for efficient long-term inhibition of saphenous vein graft failure. J Contr Release 293:172–182. https://doi.org/10.1016/j.jconrel.2018.12.001
19. Ju YM, Choi JS, Atala A et al (2010) Bilayered scaffold for engineering cellularized blood vessels. Biomaterials 31(15):4313–4321. https://doi.org/10.1016/j.biomaterials.2010.02.002
20. Zhang H, Jia X, Han F et al (2013) Dual-delivery of VEGF and PDGF by double-layered electrospun membranes for blood vessel regeneration. Biomaterials 34(9):2202–2212. https://doi.org/10.1016/j.biomaterials.2012.12.005
21. Al-Sa'doni H, Ferro A (2000) S-Nitrosothiols: a class of nitric oxide-donor drugs. Clin Sci 98(5):507–520. https://doi.org/10.1042/cs0980507
22. Naghavi N, de Mel A, Alavijeh OS et al (2013) Nitric oxide donors for cardiovascular implant applications. Small 9(1):22–35. https://doi.org/10.1002/smll.201200458
23. Joner M, Nakazawa G, Finn AV et al (2008) Endothelial cell recovery between comparator polymer-based drug-eluting stents. J Am Coll Cardiol 52(5):333–342. https://doi.org/10.1016/j.jacc.2008.04.030
24. Lipke EA, West JL (2005) Localized delivery of nitric oxide from hydrogels inhibits neointima formation in a rat carotid balloon injury model. Acta Biomater 1(6):597–606. https://doi.org/10.1016/j.actbio.2005.07.010
25. Funai EF, Davidson A, Seligman SP, Finlay TH (1997) S-nitrosohemoglobin in the fetal circulation may represent a cycle for blood pressure regulation. Biochem Biophys Res Commun 239(3):875–877. https://doi.org/10.1006/bbrc.1997.7565
26. Minamiyama Y, Takemura S, Inoue M (1997) Effect of thiol status on nitric oxide metabolism in the circulation. Arch Biochem Biophys 341(1):186–192. https://doi.org/10.1006/abbi.1997.9956
27. Bauer JA, Fung HL (1991) Chemical stabilization of a vasoactive S-nitrosothiol with cyclodextrins without loss of pharmacologic activity. Pharm Res 8:1329–1334. https://doi.org/10.1023/A:1015824417569
28. Kowaluk EA, Fung HL (1990) Dissociation of nitrovasodilator-induced relaxation from cyclic GMP levels during in vitro nitrate tolerance. Eur J Pharmacol 176:91–95. https://doi.org/10.1016/0014-2999(90)90136-T
29. Münzel T, Daiber A, Mülsch A (2005) Explaining the phenomenon of nitrate tolerance. Circ Res 97(7):618–628. https://doi.org/10.1161/01.RES.0000184694.03262.6d
30. Lautner G, Meyerhoff ME, Schwendeman SP (2016) Biodegradable poly(lactic-co-glycolic acid) microspheres loaded with S-nitroso-N-acetyl-D-penicillamine for controlled nitric oxide delivery. J Contr Release 225:133–139. https://doi.org/10.1016/j.jconrel.2015.12.056
31. Farah C, Michel LYM, Balligand JL (2018) Nitric oxide signalling in cardiovascular health and disease. Nat Rev Cardiol 15(5):292–316. https://doi.org/10.1038/nrcardio.2017.224
32. Kinlay S, Behrendt D, Wainstein M et al (2001) Role of endothelin-1 in the active constriction of human atherosclerotic coronary arteries. Circulation 104(10):1114–1118. https://doi.org/10.1161/hc3501.095707
33. Davignon J (2004) Role of endothelial dysfunction in atherosclerosis. Circulation 109(23_suppl_1):III-27-III–32
34. Drexler H (1998) Factors involved in the maintenance of endothelial function. Am J Cardiol 82(10A):3S-4S. https://doi.org/10.1016/S0002-9149(98)90420-9
35. Gimbrone MA, García-Cardeña G (2016) Endothelial cell dysfunction and the pathobiology of atherosclerosis. Circ Res 118(4):620–636. https://doi.org/10.1161/CIRCRESAHA.115.306301
36. Hansson GK (2001) Immune mechanisms in atherosclerosis. Arterioscler Thromb Vasc Biol 21(12):1876–1890. https://doi.org/10.1161/hq1201.100220
37. Steinberg D (2009) The LDL modification hypothesis of atherogenesis: an update. J Lipid Res 50(Suppl):S376–S381. https://doi.org/10.1194/jlr.R800087-JLR200